



**HAL**  
open science

## Enhanced stability of the focus obtained by wavefront optimization in dynamical scattering media

Baptiste Blochet, Kelly Joaquina, Lisa Blum, Laurent Bourdieu, Sylvain Gigan

► **To cite this version:**

Baptiste Blochet, Kelly Joaquina, Lisa Blum, Laurent Bourdieu, Sylvain Gigan. Enhanced stability of the focus obtained by wavefront optimization in dynamical scattering media. *Optica*, 2019, 6 (12), pp.1554. 10.1364/OPTICA.6.001554. hal-02400519v2

**HAL Id: hal-02400519**

**<https://hal.science/hal-02400519v2>**

Submitted on 31 Dec 2020

**HAL** is a multi-disciplinary open access archive for the deposit and dissemination of scientific research documents, whether they are published or not. The documents may come from teaching and research institutions in France or abroad, or from public or private research centers.

L'archive ouverte pluridisciplinaire **HAL**, est destinée au dépôt et à la diffusion de documents scientifiques de niveau recherche, publiés ou non, émanant des établissements d'enseignement et de recherche français ou étrangers, des laboratoires publics ou privés.

# Enhanced stability of the focus obtained by wavefront optimization in dynamical scattering media

BAPTISTE BLOCHET<sup>1,2,\*</sup>, KELLY JOAQUINA<sup>1</sup>, LISA BLUM<sup>1</sup>,  
LAURENT BOURDIEU<sup>2,†</sup>, SYLVAIN GIGAN<sup>1,†</sup>

<sup>1</sup> *Laboratoire Kastler Brossel, UPMC-Sorbonne Universités, ENS-PSL Research University, CNRS, Collège de France ; 24 rue Lhomond, F-75005 Paris, France*

<sup>2</sup> *IBENS, Département de Biologie, Ecole Normale Supérieure, CNRS, Inserm, PSL Research University, F-75005 Paris, France*

<sup>†</sup> *Senior author*

*\*baptiste.bloch@lkb.ens.fr*

**Abstract:** Focusing scattered light using wavefront shaping provides interesting perspectives to image deep in opaque samples, as e.g. in nonlinear fluorescence microscopy. Applying these techniques to in vivo imaging remains challenging due to the short decorrelation time of the speckle in depth, as focusing and imaging has to be achieved within the decorrelation time. In this paper, we experimentally study the focus lifetime after focusing through dynamical scattering media, when iterative wavefront optimization and speckle decorrelation occur over the same timescale. We show experimental situations corresponding to a broad distribution of decay rates of the scattering paths, where the focus presents significantly higher stability than the surrounding speckle.

© 2019 Optical Society of America under the terms of the OSA Open Access Publishing Agreement

## 1. Introduction

In recent years, several wavefront shaping techniques were developed to partially compensate for the scattering induced by a disordered medium and to form a diffraction limited focus using the scattered light [1], possibly at depth and non-invasively [2]. However, a major limitation to the application of these techniques to the imaging of real biological systems is the temporal decorrelation induced by minute changes of the optical index inhomogeneity: the decorrelation time of biological tissues can be in the millisecond range [3-4]. As a consequence, fast wavefront shaping systems are required for focusing light in these systems [4-5] and the lifetime of the formed focus is also limited by this decorrelation time [6]. Two main approaches have been developed to focus within this decorrelation time. On the one hand, digital optical phase conjugation (DOPC) relying on the phase conjugation of a measured wavefront is a fast non-iterative technique capable of focusing in the millisecond range [7-8]. On the other hand, iterative optimizations can focus almost as fast through a scattering medium [9-12]. While DOPC methods are very appealing to tackle fast decorrelating media, optimization methods remain inescapable in many bio-imaging scenarios, particular based on two-photon fluorescence [13-16].

So far, the lifetime of the focus obtained after wavefront shaping has only been studied for DOPC [6-7]. In particular, it has been shown experimentally and theoretically, that the temporal correlation function in intensity  $g_2(t)$ , used to quantify the decorrelation dynamics of the speckle, also gives the temporal decay of the focus intensity after phase conjugation. An analogous experiment has also been conducted with iterative optimization in the frequency domain [17], but in a stationary medium, where the decorrelation is induced by tuning the incident wavelength rather than by a physical displacement of the scatterers. In this paper, the authors demonstrated experimentally and theoretically that the focus intensity degradation is proportional to the spectral correlation function in intensity of the speckle after shifting the

laser frequency. In all these works [6, 7, 17], the medium can be considered as static during the wavefront shaping procedure, resulting in a proportionality between the timescales of speckle decorrelation and focus degradation. At the opposite, if the wavefront correction procedure is much slower than the decorrelation time, focusing of the scattered photons cannot be achieved [9].

However, an interesting question remains: what happens if we perform an iterative optimization through a dynamical scattering media, where wavefront correction and decorrelation occur over similar timescales? In this paper, we investigate which scattering medium properties (mean decorrelation time, width of the decay rate distribution) impact the characteristic lifetime of the focus obtained in such a scenario. In particular, we show that there are experimental situations where the focus can be significantly more stable than the surrounding speckle pattern, when for instance when the medium is heterogeneous. Finally, we experimentally demonstrate that this phenomenon can be observed in acute brain slices.

## 2. Principle

### 2.1 Analytical model

The output speckle pattern formed after a scattering media can be seen as a coherent sum of fields resulting from different scattering sequences (i.e. the diffusion path of a photon in the medium) with random phases and amplitudes [18]. Inside a dynamical scattering medium, each scattering sequence dephases which induce a decorrelation of the output speckle pattern. Individual scattering sequence decorrelates with a given decay rate  $\Gamma$  (see SI). Considering all scattering sequences provides the distribution of decay rates  $G(\Gamma)$  of the scattering medium [19]. This distribution can't be directly measured unlike the temporal intensity correlation function:

$$g_2(t) = \frac{\langle I(t'+t)I(t') \rangle}{\langle I(t) \rangle^2} - 1, \quad (1)$$

with  $I(t)$  the intensity of the speckle pattern measured on a camera at a time  $t$  [20-21];  $g_2(t)$  is used to characterize the temporal decorrelation of these sequences.  $G(\Gamma)$  and  $g_2(t)$  can be linked by the following equation [19] (see SI):

$$g_2(t) = \left| \int G(\Gamma) \cdot \exp(-\Gamma \cdot t) d\Gamma \right|^2. \quad (2)$$

For example, the inverse of the slope at the origin of this function (up to a prefactor) gives the mean decorrelation time  $\tau$ , which is the mean time over which the scattering sequences change [19, 22]. A full analysis of the autocorrelation function can provide higher moments of the distribution of decay rates.

In the specific case of a monodisperse colloidal solution, the decay rate of a scattering path is proportional to the number of scattering events encountered. So the distribution of decay rates is directly proportional to the path length distribution [18]. For more complex scattering media, for example where some parts are static and others are moving or when the distribution of scatterer size isn't known (biological tissue), there is no simple relation between these two quantities.

Performing wavefront shaping with a spatial light modulator (SLM) means adding the appropriate phase to the incident wavefront to sum constructively some sequences at a desire target to form a sharp focus. Inside a dynamic scattering media, the scattering sequences dephase which induce a degradation of the focus after ending wavefront shaping. The normalized degradation of the focus can be expressed in a similar way than equation 2 (see SI):

$$I_{\text{focus}}(t) = \left| \int G_m(\Gamma) \cdot \exp(-\Gamma \cdot t) d\Gamma \right|^2. \quad (3)$$

With  $G_m(\Gamma)$  the distribution of decay rates of the focus. If the sequences selected to focus through a dynamical scattering medium present the same decay rate distribution as the full set of sequences forming the speckle, the focus and the speckle should have the same decorrelation

dynamics, as it was observed in DOPC. Hypothetically, if more stable scattering sequences could be favored during wavefront shaping (by selecting either more stable scatterers or shorter sequences), the focus should present a higher stability than the initial speckle before optimization.

For a continuous iterative optimization, if decorrelation and optimization occur over similar timescales, it is not clear which scattering sequences will be used to form a focus. We experimentally investigate this question with a custom fast wavefront shaping system [9]. We use this setup to focus through synthetic homogeneous scattering media of various stabilities and scattering strengths, but also stratified media with a “static” and a “dynamic” part, as it can be the case for biological samples. In this latter case, the width of the decay rate distribution of the different scattering sequences in the medium can be broad. We study the degradation of the focus in these various scenarios and investigate under which conditions the focus could present an enhanced stability.

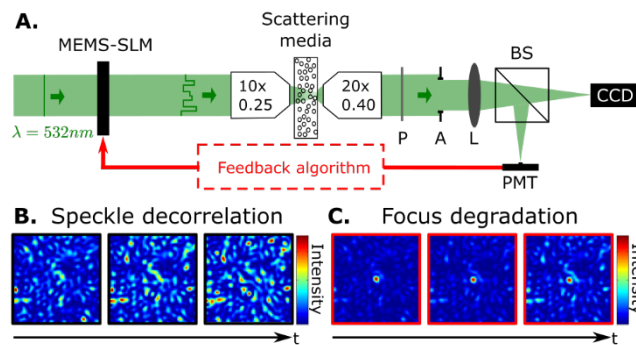


Fig. 1. (A) Experimental setup. P: polarizer; A: aperture; L: lens (focal length = 150mm); BS: beamsplitter; MEMS-SLM; MEMS-based spatial light modulator. The wavefront of a collimated laser beam ( $\lambda=532\text{ nm}$ ) is modulated by a phase-only spatial light modulator. The phase mask is imaged on the back aperture of a microscope objective and focused into a scattering sample. A second microscope objective images the output speckle using a beamsplitter on a CCD camera and on a PMT. The PMT collects the intensity of one speckle grain through an optical fiber. A polarizer selects one polarization state of the output speckle. The PMT signal is acquired by a DAQ board and sent to a FPGA board. During the optimization algorithm, the FPGA board computes the optimal phase for a given Hadamard mode, adds it to the current phase mask of the SLM and applies the new mask to the SLM. Optimization of one mode takes  $243\ \mu\text{s}$ . (B) A stack of speckle patterns is recorded over time to characterize the decorrelation dynamics of the speckle. (C) After ending the optimization, the focus degrades in time due to the speckle decorrelation.

## 2.2 Experimental setup

Fig. 1 describes the experimental wavefront shaping setup. A phase only spatial light modulator (Kilo-DM segmented, Boston Micromachines) shapes the incident wavefront of a CW laser  $\lambda=532\text{ nm}$  (Coherent Sapphire). The SLM is conjugated to the back focal plane of a microscope objective (10x, 0.25), which illuminates a scattering sample. The polarized output speckle is simultaneously imaged onto a CCD camera (Allied Vision Technologies Manta G-046B) and on a mono-detector (PMT, Hamamatsu H10721-20). A continuous iterative wavefront optimization algorithm is implemented to maximize the intensity of one speckle grain collected by the PMT. In short, the optimization is obtained using the Hadamard input basis. At each iteration, half of the pixels are modulated in phase, while the PMT signal is monitored, and the optimal phase is added to the correction mask. We combined a fast acquisition card (NI PXIe-6361) and a fast FPGA board (NI PXIe-7962R) to reach a speed of 4,1 kHz per mode [9]. For all of experiments, the full Hadamard basis is successively optimized 5 times in 1.25 s.

Our experimental system is capable of measuring successively the temporal correlation function in intensity  $g_2(t)$  and the focus degradation after ending the optimization  $I_{\text{focus}}(t)$ . Indeed, the PMT signal provides  $I_{\text{focus}}(t)$  and  $g_2(t)$  is measured with the CCD camera [20-21].

### 2.3 Fitting model

Establishing a complete theory describing which dynamic scattering sequences are selected during an iterative optimization to focus remains difficult and outside of the scope of this article. Instead, we use a simple analysis of our experimental results. As was done previously to quantify the  $g_2$  function [19], we express both decorrelation functions (of the speckle  $g_2$  and of the focus  $I_{\text{focus}}$ ) as a function of the moments of their decay rate distribution:

$$g_2(t) \text{ or } I_{\text{focus}}(t) = \alpha + (1 - \alpha) \times \exp\left(\frac{-2t}{\tau}\right) \times \left(1 + t^2 \frac{\sigma_{\tau}^2}{2}\right)^2 \quad (4)$$

with  $\tau$  the mean decorrelation time,  $\alpha$  a correlation term at large times that results from the presence of static sequences and  $\sigma_{\tau}$  the standard deviation of the decay rate distribution. Each of these 3 quantities are defined respectively for the decorrelation of the speckle and of the focus. Additional moments could be added to this expression but they are, experimentally, harder to extract due to noise.

Therefore, we can compare for all experiments the decay rate distribution (through the estimate of its mean value and its standard deviation) for the speckle and the focus. If the focus uses statistically the same scattering sequences as the speckle, these distributions (and therefore their first moments) should be identical. On the other hand, if more stable scattering sequences are favored during wavefront shaping the mean value of the decay rate distribution of the focus should be higher and the width of its distribution should be narrower. Moreover, if the medium contains static scattering sequences, and if they are favored by the wavefront shaping optimization, the correlation term at large times  $\alpha$  will be larger for the focus.

## 3. Results

We have used different samples in order to understand in which situation a stable focus can be formed. We studied first the case of a colloidal solution in multiple scattering regime, where difference of sequence decay rate results from difference in their length. The width of the path length distribution of such a medium (and therefore its decay rate distribution) is not tunable. To study the impact of the width of the decay rate distribution, we then designed a second category of samples, composed of a thin dynamical layer above a static layer in multiple scattering regime. In this medium, part of the light travels ballistically through the dynamical layer. Therefore, static scattering sequences exist through the sample. By varying the size of the scatterers inside the colloidal solution, the decay rate distribution of the dynamical scattering sequences could be tuned. For small polystyrene beads, scattered light was highly unstable. In this situation our optimization scheme was only capable of compensating for the static sequences. On the other hand, for large polystyrene beads, the decorrelation was slower. In this last situation, our system was both capable of compensating static and dynamical scattering. Finally, we achieved qualitatively the same result through acute brain slices from the brainstem.

### 3.1 Monodisperse colloidal solution

The first sample used was a 500  $\mu\text{m}$  thick solution of  $\text{TiO}_2$  (Sigma Aldrich 224227) in glycerol with a mass concentration of 20 g/l ( $\ell_s = 70 \mu\text{m}$  and  $l^* = 200 \mu\text{m}$ ) [9]. Light propagation through the sample is therefore in a regime of multiple scattering. A schematic of a few dynamical sequences is illustrated in fig 2.a. The decorrelation time of a scattering sequence in a monodisperse solution is directly related to the number of scattering events [18]. Furthermore, tuning the temperature modifies the viscosity of the sample, thus allowing to tune its mean decorrelation time.

The temperature of the sample was first adjusted at 16 ° C to obtain an average decorrelation time of the speckle of  $\tau_{\text{speckle}} = 70$  ms. The resulting mean focus degradation and its standard deviation are shown on fig 2.b. For this dynamical sample, a mean focus decorrelation time of  $\tau_{\text{focus}} = 70$  ms with a standard deviation of 21 ms was measured over 500 realizations.

We then measured the average value of the focus decorrelation time and its standard deviation for different media, obtained by changing the viscosity of the solution via the sample temperature, such that the decorrelation time of the speckle was ranging from 50 ms to 150 ms. In fig. 2.c, the ratio  $\tau_{\text{focus}} / \tau_{\text{speckle}}$  is shown. This ratio is constant and close to unity for all tested stabilities. Interestingly, an individual realization of the focus may have a characteristic decorrelation time different from the one of the speckle, but on average they are identical. We also didn't measure any significant difference between the standard deviation of the decay rate distribution of the focus and of the speckle for these experiments. For those samples, this value was ranging from  $1 \cdot 10^{-3} \text{ ms}^{-1}$  to  $3 \cdot 10^{-3} \text{ ms}^{-1}$ . Considering all experiments, the mean  $R^2$  obtained by fitting  $g_2$  was  $0.99 \pm 0.01$ . The mean  $R^2$  obtained by fitting each individual focus decorrelation was  $0.96 \pm 0.01$ . This lower value originates from the dynamic speckle background that overlaps with the focus. A residual offset  $\alpha$  of the order of 1% can be measured in those experiments. It results from imperfection in the measurements: finite FOV on the camera to measure  $g_2$  and insufficient averaging to remove the speckle background for the focus. This residual offset is of the order of the fit accuracy and was therefore neglected.

So far, using monodisperse colloidal solutions, we didn't find any optimization procedures that may favor stable scattering sequences. The decay rate distribution might be too narrow to observe different stabilities between the focus and the speckle. To investigate further, we synthesized dynamical scattering media with a wider decay rate distribution of the different scattering sequences.

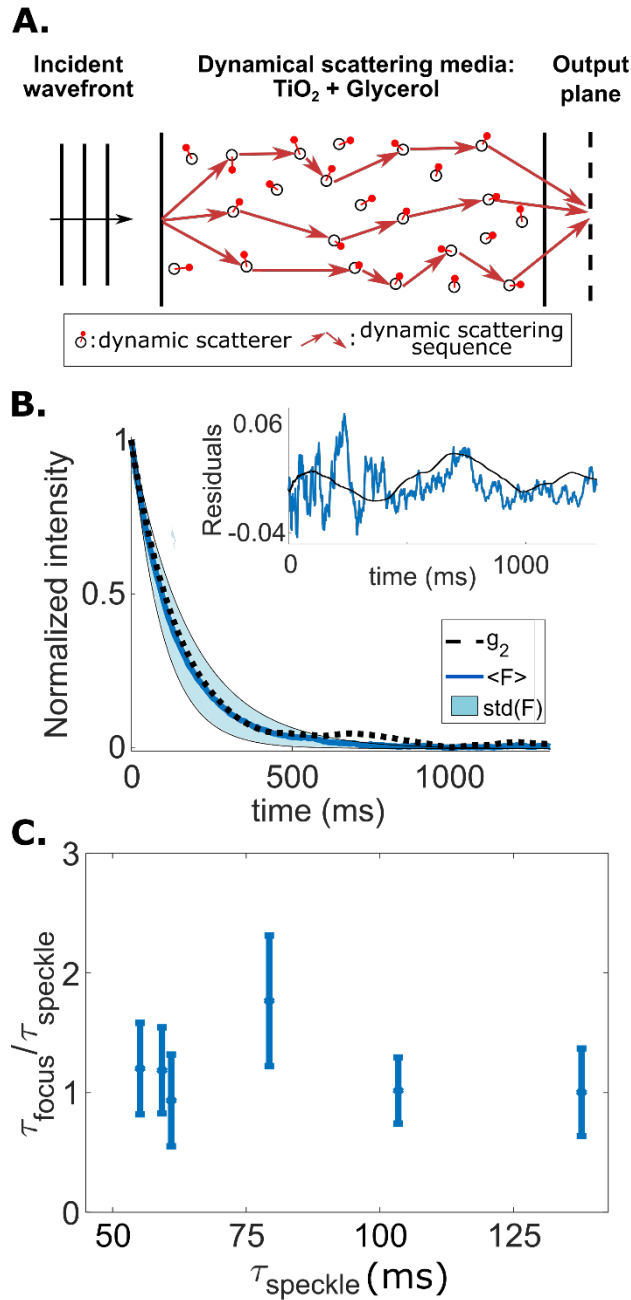


Fig 2. Focus stability through a monodisperse colloidal solution. (A) Scheme of the scattering process. When propagating inside a scattering medium, light will travel through many scattering sequences and will then interfere to form a speckle pattern. For a dynamical medium, sequences will change in time leading to the decorrelation of the speckle. (B) Evolution in time of the focus after ending the optimization through a medium with a mean decorrelation time of 70 ms: average (solid line) and standard deviation (blue region) over 500 realizations. Dotted line: intensity correlation function ( $g_2$ ) of the speckle. Averaged over a large number of realizations, the focus presents the same stability as the speckle, even if each individual realization doesn't. Inset: Residuals of the fit of  $g_2$  (dark line) and of an individual focus degradation (blue) (C) Ratio of the focus mean decorrelation time and of the speckle decorrelation time for different speckle

decorrelation times. In average, the focus presents the same stability as the speckle through a monodisperse colloidal solution.

### 3.2 Combination of layers of static and dynamic scatterers

In a second experiment, we synthesized dynamical scattering media that exhibits a larger decay rate distribution (see Figure 3.a for a diagram of the scattering sequences existing in our media). By superimposing two scattering media, a thick static layer and a thin dynamical layer, we were able to control the percentage of dynamical scattering sequences exiting the sample. In this experiment, we wanted to investigate which sequences (fixed or dynamic and which ones among the dynamic) will form a focus after optimization. In a first experimental situation, we designed a sample where the dynamical sequences were decorrelating too fast to be corrected by our wavefront shaping system. In a second situation, we designed a sample where the dynamical sequences were slower and may be compensated by our system [9].

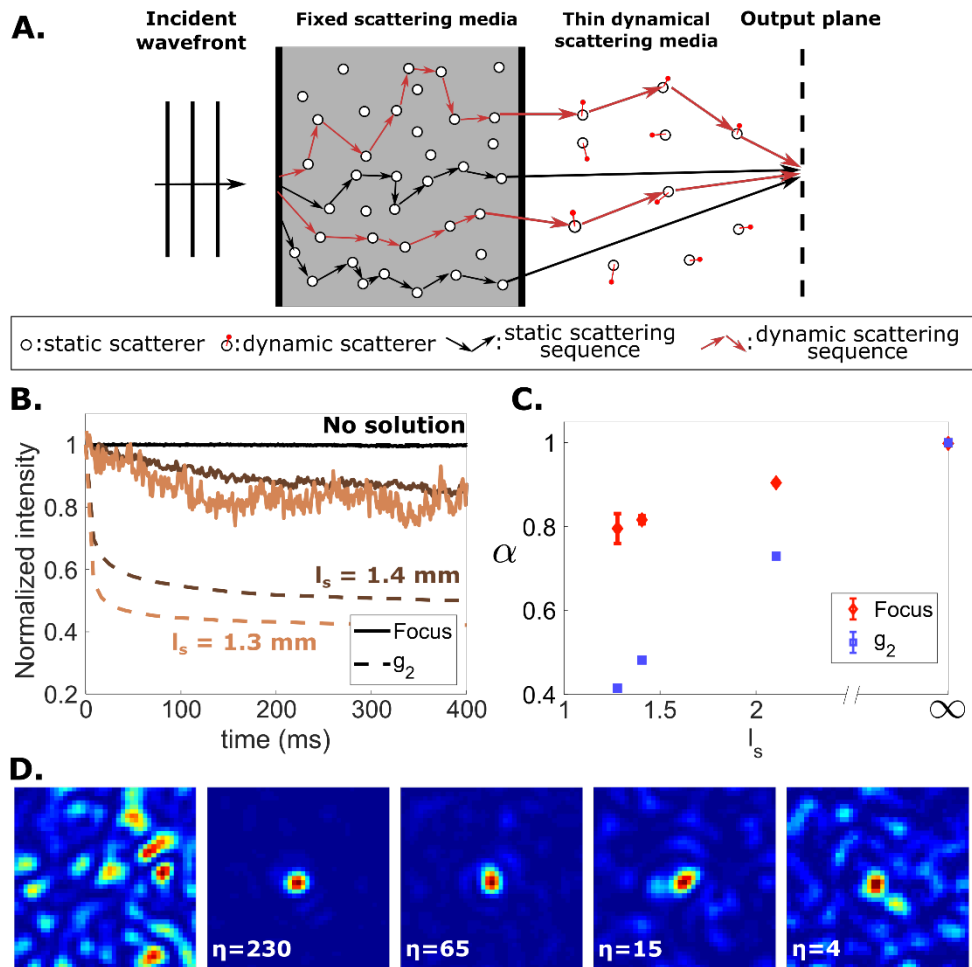


FIG 3. Focusing through two layers of scattering media (a static scattering medium and a fast dynamical scattering medium) (A) Scheme of the scattering sample. Light is first multiply scattered by a fixed scattering layer (in grey). Then light encounters only few scattering events by propagating through a dynamical scattering layer. Part of the light propagates ballistically through this dynamical layer (black arrows); the other sequences (in red) decorrelate due to the motion of the scatterers. (B) Comparison between focus degradation (solid lines) and speckle decorrelation (dotted lines) for different scattering mean free paths of the colloidal solution. The

mean speckle decorrelation time, in presence of the colloidal solution, is below 1 ms. The optimization process isn't fast enough to compensate for this dynamical scattering. Therefore, the sequences contributing to the focus are mostly static sequences. (C) Mean value of the plateau  $\alpha$  after decorrelation for the focus (red diamonds) and the speckle (blue square) for different scattering mean free path of the colloidal solution. Error bars represent the 95% confidence bounds of the fit. (D) CCD images ( $320 \times 320 \mu\text{m}^2$ ) of the speckle pattern measured before optimization (left) and after a stable focus is obtained for different scattering samples (from left to right:  $\ell_s = \infty$ , 2.1 mm, 1.4 mm, 1.2 mm).

The first medium was a solution of polystyrene beads (Polybead® Carboxylate Microspheres  $0.35 \mu\text{m}$ ) in water positioned over a thick static scattering medium. The thickness of the layer of the dynamical scattering solution was 1 mm.

The percentage of ballistic photons through the scattering solution was controlled by adjusting the polystyrene beads concentration. Using Mie theory, the concentration required to obtain a given mean free diffusion path in the dynamical medium can be computed. This percentage ranges from 46% ( $\ell_s = 1.3 \text{ mm}$ ) to 100% (no scattering solution). The addition of a strongly scattering static layer ensures that we are overall in the multiply scattering regime.

For each solution, the measurement of  $g_2$  confirms that the speckle resulting from dynamically scattered photons decorrelates in less than a millisecond (see Figure 3.b, dashed lines). We also observe that the  $g_2$  function reaches a plateau ( $\alpha_{\text{speckle}}$ ) for large decorrelation times, indicating that static sequences contribute to the speckle pattern. For each sample, the decorrelation of the focus averaged over 100 realizations is plotted in Figure 3.b (solid line). Yet, for all tested concentrations of colloidal solutions (figure 3.b), the wavefront correction system was able to form a focus, which was decorrelating slower than the speckle and was eventually reaching a plateau. As our system is not fast enough to compensate for the dynamically scattered photons, the value of the plateau ( $\alpha_{\text{focus}}$ ) was larger than the one measured for the speckle ( $\alpha_{\text{speckle}}$ ), showing that the focus contains a larger amount of static sequences (figure 3.b). As the scattering mean free path decreases, more and more photons were scattered by the dynamical layer (figure 3.c). Nevertheless, in all cases, the focus obtained by wavefront shaping was mostly formed by static scattering sequences. Interestingly, some slowly decorrelating (in the order of the second) scattering sequences are also contributing to the focus. These more stable sequences are probably snake-like sequences that encounter only very few forward scattering events. Finally, we have seen that, through these samples, the mode distribution used to form a focus is very different from the one of the speckle. Moreover, figure 3.d shows that the enhancement of the focus intensity by optimization (as defined in Vellekoop et al [23]) was larger for smaller bead concentrations in the dynamical samples. Indeed, the dynamical scattering speckle can be seen as an extra measurement noise that reduces the enhancement [24].

We then synthesized a similar dynamical medium but with larger colloidal beads (Polybead® Carboxylate Microspheres  $1 \mu\text{m}$ ). The larger beads sustained higher viscosity forces, which decreased the decay rates of the dynamical scattering sequences. By tuning the concentration (therefore  $\ell_s$ ), we simultaneously controlled the percentage of fixed sequences that exited from the sample and the mean decorrelation time of the dynamical sequences. For all prepared samples, the mean speckle decorrelation times ranged from 50 ms to 250 ms and the proportion of fixed scattering sequences ranged from almost 0 to 80%. Our wavefront shaping system should therefore be capable of optimizing the phase of the wavefront travelling through any of these sequences [9]. The standard deviation the decay rate distribution ranged from  $2 \cdot 10^{-3} \text{ ms}^{-1}$  to  $11 \cdot 10^{-3} \text{ ms}^{-1}$ .

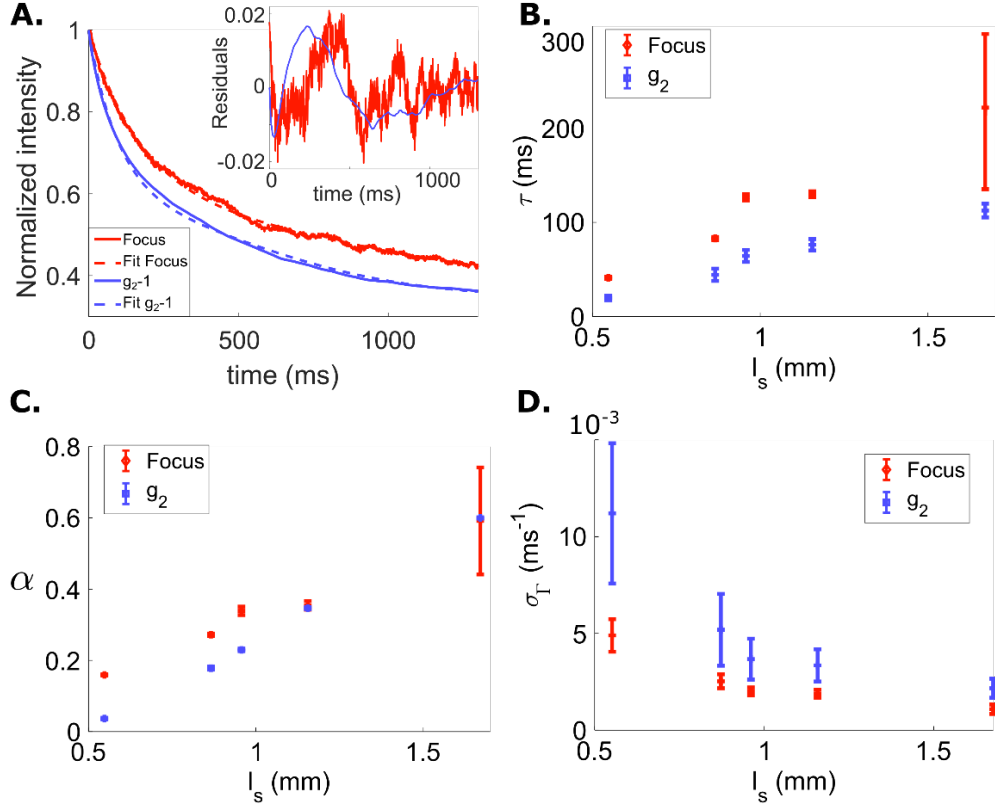


Fig 4. Focusing through two layers of scattering media (a static medium and a slow dynamical scattering medium). The scheme of the experiment is similar to the one shown on Fig. 3. The dynamical scattering medium is an aqueous colloidal solution of polystyrene beads. Due to larger polystyrene beads, the mean scattering decorrelation time is slower ranging from 55 ms to 405 ms, as compared to the case shown in Fig. 3. Here, the optimization procedure is fast enough to compensate for the dynamical scattering. (A) Example of a focus degradation (red line) and speckle decorrelation (blue line) for a colloidal solution with  $\ell_s = 0.6$  mm. Inset Residuals of the fits. (B) Mean decorrelation of the focus (red diamonds) and mean decorrelation time of the speckle (blue squares) for different scattering mean free paths of the colloidal solution. Error bars represent the 95% confidence bounds of the fit. In average, the focus is two times more stable than the focus. (C) Mean position of the plateau  $\alpha$  after decorrelation for the speckle (blue squares) and for the focus (red diamonds), for different scattering mean free path of the colloidal solution. Error bars represent the 95% confidence bounds of the fit. (D) Standard deviation of the decay rate distribution for the speckle (blue squares) and for the focus (red diamonds). The scattering sequences contributing to the focus are the more stable one. Their distribution is also narrower compare to the initial speckle decay rate distribution.

The results are presented in figure 4 for  $\ell_s$  ranging from 0.6 mm to 2.3 mm. Examples of focus and speckle decorrelation are presented in figure 4.a for  $\ell_s = 0.6$  with their fits and residuals. Considering all experiments, the mean  $R^2$  obtained was  $0.97 \pm 0.01$ . The blue squares and the red diamonds indicate the average proportion of static sequences (fig 4.b) the mean decorrelation time (fig 4.c) and the standard deviation of the decay rate distribution (fig 4.d) respectively for the speckle and the focus. The data obtained for the focus were averaged over 100 realizations.

For large  $\ell_s$ , most of the scattering sequences inside the scattering medium are static. Therefore, there is not much possibility of increasing the number of static scattering sequences contributing to the focus. For small  $\ell_s$ , the proportion of static sequences increases at the focus. In all cases, the focus exhibits, in average, a two-fold higher mean decorrelation time as compared to the speckle, which also results in a narrower width of the decay rates distribution

for the focus. In a monodisperse colloidal scattering solution, these more stable sequences should correspond to snake-like sequences that encounter only few forward scattering events. The intensity enhancement as defined in Vellekoop et al [23], follows a linear trend similar to the one previously reported [9] ranging from 20 for  $\tau_{\text{speckle}} = 25$  ms to 120 for  $\tau_{\text{speckle}} = 225$  ms.

To conclude, the key element to form a focus with stable sequences seems to be the width of the decay rate distribution of the different scattering sequences. The broader the distribution of the different scattering sequences is, the more stable sequences the focus contains and the larger its lifetime.

### 3.3 Biological samples

As a last experiment, we investigated whether our optimization algorithm allows achieving in biological tissues a focus more stable than the speckle [25]. This would of course be very beneficial to perform non-linear imaging after wavefront correction, since an increased focus stability would provide additional time for the formation of a fluorescence image.

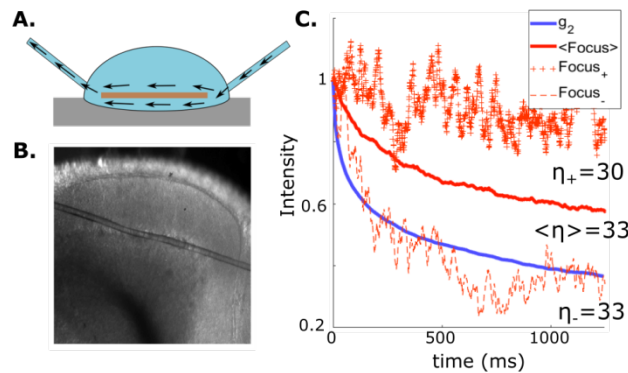


Fig 5. (A) Scheme of the setup to maintain acute brain slices. A slice is immersed in an oxygenized buffer which is renewed with a flux. (B) Oblique wide field image ( $4.6 \times 4.6 \text{ mm}^2$ ) of a typical acute brain slice (cerebellum). (C) Focusing through an acute mouse brain slice of  $300 \mu\text{m}$ . Intensity correlation of the speckle: blue; average focus degradation (red,  $\langle \text{Focus} \rangle$ ), more stable degradation ( $\text{Focus}_+$ ) and less stable degradation ( $\text{Focus}_-$ ). The scattering sequences show a fast decorrelation ( $\sim 100$  ms) followed by a slow one ( $\sim 5$  s). In average the optimization process promotes the most stable sequences at the focus. In the best case, the focus is only formed with stable sequences. On the contrary, in the worst case, the focus degradation follows the speckle decorrelation.

Our sample was a  $300 \mu\text{m}$  thick acute slice of mouse brain ( $l_s \sim 40 \mu\text{m}$  [26]). To keep the slices alive, a stream of a solution of 125 mM NaCl, 2.5 mM KCl, 2 mM  $\text{CaCl}_2$ , 1 mM  $\text{MgCl}_2$ , 1.25 mM  $\text{NaH}_2\text{PO}_4$ , 26 mM  $\text{NaHCO}_3$  and 25 mM glucose, bubbled with 95%  $\text{O}_2$  and 5%  $\text{CO}_2$ , was imposed around the wafer [27]. Every effort has been made to keep the brain slices alive for the duration of the experiment. The scheme of the system used to maintain the slice acute is shown on fig. 5.a and a typical widefield image of a slice is shown on fig. 5.b.

Figure 5.c shows (solid blue line) the temporal correlation function of the speckle. A first rapid decorrelation (slope at the origin of  $\sim 100$  ms) is followed at long times by a slower decorrelation with a typical timescale of the order of 5 s. We did not study here the microscopic origin of these different decorrelation times. As in the previous experiment, we observed that the focus obtained by optimization (solid red line) is on average (over 500 realizations) more stable than the speckle and presents an average enhancement of  $33 \pm 10$ . The red dotted line and the red crossed line show respectively the least stable focus and the most stable focus. These two optimizations led to identical enhancement of the order of 30. It seems that there are no benefits (or drawbacks) in term of enhancement to favor stable sequences. Interestingly, the most stable focus generated here seems to be almost perfectly stable (over tens of seconds).

#### **4. Discussion and conclusion**

We have shown that, in contrast with previous wavefront shaping experiments, the focus does not always have the same decay rate distribution as the surrounding speckle. We have shown in particular that in specific conditions an increase of the focus mean decorrelation time by a factor 2 (Fig. 4) up to several orders of magnitude (Fig. 3) is obtained, as compared to the speckle stability.

Our interpretation of this results is the following. At each iteration of the optimization, some stable and dynamic sequences are corrected to interfere constructively to the focus. Rapidly, the dynamic sequences decorrelate and do not contribute to the focus anymore, while the stable sequences still do. Therefore, iteration after iteration, more and more stable sequences accumulate leading to an enhanced stability of the focus. Ultimately, all the SLM mode available could compensate only for the stable sequences (as observed in Fig. 5.c). The key to achieve a more stable focus seems to be the width of the decay rate distribution of the scattering sequences. The wider this distribution, the easier it is to promote stable diffusion sequences by optimization. On the contrary, a narrow distribution (as through a monodisperse solution) did not allow, for an iterative optimization of the wavefront, the selection of more stable sequences, at least for the range of parameters investigated. Another key element to obtain a more stable focus is the speed at which the optimization is done. If the optimization is too fast compared to the decorrelation time of the medium, this effect does not appear (as in DOPC). In our case, we observed that if the optimization time is of the order of the mean decorrelation time of the medium, a focus more stable than the speckle can be formed. The influence of these two parameters (width of the decay rate distribution of the scattering sequences, speed at which the optimization is done) remains difficult to analyze experimentally and further numerical studies (beyond the scope of this paper) may be required to fully describe their respective role. Additional studies of the impact of the optimization algorithm on the stability of the focus could highlight optimization strategies that can further promote the emergence of a more stable focus.

We believe these results are of great interest particularly for biomedical imaging. For instance, during *in vivo* imaging of a mouse brain (the skull having been removed and replaced by a glass coverslip), part of the light propagates through or around blood vessels, thus imposing a very rapid decorrelation of the speckle. Despite this, a wavefront correction system should be able to focus the photons scattered by static structures or having a slow dynamic (cells, myelinated axons, ...), if the fraction of dynamically scattered light remains low. Another important scenario is imaging through the skull. The skull would then act as a nearly static scatterer and the brain tissue would be the dynamical one. In this case, we expect the wavefront correction system to preferentially correct the scattering by the skull. An interesting case is the correction of the wavefront in the presence of a ballistic but aberrant wavefront inside a tissue. The scattered light rapidly decorrelates whereas the aberrated light will be relatively stable. A correction of the wavefront would then preferentially correct aberrations. One last perspective could be to extend this study to the broadband regime. Mounaix et al demonstrated a selection of short scattering sequences by exploiting the short coherence length of a pulsed laser through a homogeneous scattering media [28]. By exploiting this effect, one could obtain a further increase in the stability of the focus.

#### **5. Funding,**

H2020 European Research Council (ERC) (278025, 724473); Université Pierre et Marie Curie (UPMC); Agence Nationale de la Recherche (ANR-15-CE19-0011-01 and ANR-15-CE19-0011-03 ALPINS, ANR-10-LABX-54 MEMOLIFE, ANR-10-IDEX-0001-02 PSL\* Research University and ANR-10-INSB-04-01 France-BioImaging infrastructure.

#### **6. Acknowledgments**

We thank Claudio Moretti, Dimitri Dumontier, Stephane Dieudonné and Mariano Casado for valuable help with the acute brain slices experiment and Cathie Ventalon for advices and comments on the project. S. G. is a member of the Institut Universaire de France. B. B. was funded by a Ph.D. fellowship from UPMC under the program “Interface pour le Vivant”.

## References

1. Rotter, S., & Gigan, S. (2017). Light fields in complex media: Mesoscopic scattering meets wave control. *Reviews of Modern Physics*, 89(1), 015005.
2. Horstmeyer, R., Ruan, H., & Yang, C. (2015). Guidestar-assisted wavefront-shaping methods for focusing light into biological tissue. *Nature photonics*, 9(9), 563.
3. Qureshi, M. M., Brake, J., Jeon, H. J., Ruan, H., Liu, Y., Safi, A. M., ... & Chung, E. (2017). In vivo study of optical speckle decorrelation time across depths in the mouse brain. *Biomedical optics express*, 8(11), 4855-4864.
4. Liu, Yan, et al. "Optical focusing deep inside dynamic scattering media with near-infrared time-reversed ultrasonically encoded (TRUE) light." *Nature communications*6 (2015): 5904.
5. Stockbridge, C., Lu, Y., Moore, J., Hoffman, S., Paxman, R., Toussaint, K., & Bifano, T. (2012). Focusing through dynamic scattering media. *Optics express*, 20(14), 15086-15092.
6. Jang, M., Ruan, H., Vellekoop, I. M., Judkewitz, B., Chung, E., & Yang, C. (2015). Relation between speckle decorrelation and optical phase conjugation (OPC)-based turbidity suppression through dynamic scattering media: a study on in vivo mouse skin. *Biomedical optics express*, 6(1), 72-85.
7. Liu, Y., Ma, C., Shen, Y., Shi, J., & Wang, L. V. (2017). Focusing light inside dynamic scattering media with millisecond digital optical phase conjugation. *Optica*, 4(2), 280-288.
8. Wang, D., Zhou, E. H., Brake, J., Ruan, H., Jang, M., & Yang, C. (2015). Focusing through dynamic tissue with millisecond digital optical phase conjugation. *Optica*, 2(8), 728-735.
9. Blochet, B., Bourdieu, L., & Gigan, S. (2017). Focusing light through dynamical samples using fast continuous wavefront optimization. *Optics letters*, 42(23), 4994-4997.
10. Cui, M. (2011). A high speed wavefront determination method based on spatial frequency modulations for focusing light through random scattering media. *Optics express*, 19(4), 2989-2995.
11. Feldkhun, D., Tzang, O., Wagner, K. H., & Piestun, R. (2019). Focusing and scanning through scattering media in microseconds. *Optica*, 6(1), 72-75.
12. Tzang, O., Niv, E., Singh, S., Labouesse, S., Myatt, G., & Piestun, R. (2018). Wavefront shaping in complex media at 350 KHz with a 1D-to-2D transform. *arXiv preprint arXiv:1808.09025*.
13. Tang, J., Germain, R. N., & Cui, M. (2012). Superpenetration optical microscopy by iterative multiphoton adaptive compensation technique. *Proceedings of the National Academy of Sciences*, 109(22), 8434-8439.
14. Papadopoulos, I. N., Jouhanneau, J. S., Poulet, J. F., & Judkewitz, B. (2017). Scattering compensation by focus scanning holographic aberration probing (F-SHARP). *Nature Photonics*, 11(2), 116.
15. Galwaduge, P. T., Kim, S. H., Grosberg, L. E., & Hillman, E. M. C. (2015). Simple wavefront correction framework for two-photon microscopy of in-vivo brain. *Biomedical optics express*, 6(8), 2997-3013.
16. Ji, N., Milkie, D. E., & Betzig, E. (2010). Adaptive optics via pupil segmentation for high-resolution imaging in biological tissues. *Nature methods*, 7(2), 141.
17. Van Beijnum, F., Van Putten, E. G., Lagendijk, A., & Mosk, A. P. (2011). Frequency bandwidth of light focused through turbid media. *Optics letters*, 36(3), 373-375.
18. Maret, G., & Wolf, P. E. (1987). Multiple light scattering from disordered media. The effect of Brownian motion of scatterers. *Zeitschrift für Physik B Condensed Matter*, 65(4), 409-413.
19. Frisken, Barbara J. "Revisiting the method of cumulants for the analysis of dynamic light-scattering data." *Applied optics* 40.24 (2001): 4087-4091
20. Wong, A. P., & Wiltzius, P. (1993). Dynamic light scattering with a CCD camera. *Review of Scientific Instruments*, 64(9), 2547-2549.
21. Viasnoff, V., Lequeux, F., & Pine, D. J. (2002). Multispeckle diffusing-wave spectroscopy: A tool to study slow relaxation and time-dependent dynamics. *Review of scientific instruments*, 73(6), 2336-2344.
22. Savo, R., Pierrat, R., Najar, U., Carminati, R., Rotter, S., & Gigan, S. (2017). Observation of mean path length invariance in light-scattering media. *Science*, 358(6364), 765-768.
23. Vellekoop, Ivo M., and A. P. Mosk. "Focusing coherent light through opaque strongly scattering media." *Optics letters* 32.16 (2007): 2309-2311.
24. Vellekoop, I. M., & Mosk, A. P. (2008). Phase control algorithms for focusing light through turbid media. *Optics communications*, 281(11), 3071-3080.
25. Brake, J., Jang, M., & Yang, C. (2016). Analyzing the relationship between decorrelation time and tissue thickness in acute rat brain slices using multispeckle diffusing wave spectroscopy. *JOSA A*, 33(2), 270-275.
26. Jacques, S. L. (2013). Optical properties of biological tissues: a review. *Physics in Medicine & Biology*, 58(11), R37.
27. Paoletti, P., Ascher, P., & Neyton, J. (1997). High-affinity zinc inhibition of NMDA NR1–NR2A receptors. *Journal of Neuroscience*, 17(15), 5711-5725.
28. Mounaix, M., de Aguiar, H. B., & Gigan, S. (2017). Temporal recompression through a scattering medium via a broadband transmission matrix. *Optica*, 4(10), 1289-1292.

# Enhanced stability of the focus obtained by wavefront optimization in dynamical scattering media: supplementary material

BAPTISTE BLOCHET<sup>1,2,\*</sup>, KELLY JOAQUINA<sup>1</sup>, LISA BLUM<sup>1</sup>, LAURENT BOURDIEU<sup>2,†</sup>, SYLVAIN GIGAN<sup>1,†</sup>

<sup>1</sup>Laboratoire Kastler Brossel, UPMC-Sorbonne Universités, ENS-PSL Research University, CNRS, Collège de France ; 24 rue Lhomond, F-75005 Paris, France

<sup>2</sup>IBENS, Département de Biologie, Ecole Normale Supérieure, CNRS, Inserm, PSL Research University, F-75005 Paris, France

<sup>†</sup>Senior author

\*Corresponding author: [baptiste.bloch@lkb.ens.fr](mailto:baptiste.bloch@lkb.ens.fr)

Published XX Month XXXX

This document provides supplementary information to “Enhanced stability of the focus obtained by wavefront optimization in dynamical scattering media”. It shows the derivation of two models to express the autocorrelation function  $g_1$  and the degradation of the focus after wavefront shaping as integrals of exponential decay over decay rate distributions.

<http://dx.doi.org/10.1364/optica.99.099999.s1> [supplementary document doi]

## Supplementary 1: Autocorrelation function and decay rate distribution

Under the diffusion approximation, we can write that the total field at the detector is a superposition of the fields from all light paths through the sample to the detector:

$$E(t) = \sum_p E_p e^{i\varphi_p(t)} \quad (\text{S1.1})$$

where  $\sum_p$  represents the sum over paths,  $E_p$  and  $\varphi_p$  are respectively the amplitude and the phase of the field from path  $p$ .

By assuming that the fields from different paths are uncorrelated, we obtain:

$$g_1(t) \equiv \frac{\langle E(t')E^*(t+t') \rangle}{\langle |E(t)|^2 \rangle} = \sum_p \frac{|E_p|^2}{\langle I \rangle} \langle e^{i\Delta\varphi_p(t)} \rangle \quad (\text{S1.2})$$

Where  $\langle I \rangle$  is the total average scattered intensity at the detector and  $\Delta\varphi_p(t) = \varphi_p(0) - \varphi_p(t)$ . Using the fact that  $\Delta\varphi_p$  is a gaussian random variable, we obtain:

$$\langle e^{i\Delta\varphi_p(t)} \rangle = e^{-\langle \Delta\varphi_p(t)^2 \rangle / 2} \quad (\text{S1.3})$$

For a mixture of colloidal scatterers under Brownian motion, we obtain the following expression [1]:

$$\langle \Delta\varphi_p(t)^2 \rangle = \sum_i 2n_{i,p} \langle q_{i,p}^2 \rangle D_{i,p} t \quad (\text{S1.4})$$

where  $\sum_i$  represents the sum over particle type,  $n_{i,p}$  the number of scattering events from specie  $i$ ,  $\langle q_{i,p}^2 \rangle$  the average over scattering vectors and  $D_{i,p}$  the diffusing constant of the specie  $i$  in the path  $p$ .

We can now express the autocorrelation function in the following way:

$$g_1(t) = \sum_p \frac{|E_p|^2}{\langle I \rangle} e^{-\Gamma_p t} \quad (\text{S1.5})$$

Where  $\Gamma_p = \sum_i 2n_{i,p} \langle q_{i,p}^2 \rangle D_{i,p}$  is the decay rate associated to the path  $p$ . We can recast the last equation as a sum over decay rates  $\Gamma$  rather than a sum over individual paths provided that we replace the fraction of scattered intensity in path  $p$ :  $|E_p|^2 / \langle I \rangle$ , with the distribution of decay rates  $G(\Gamma)$ :

$$g_1(t) = \sum_\Gamma G(\Gamma) e^{-\Gamma t} \quad (\text{S1.6})$$

By passing to the continuum limit, we finally obtain:

$$g_1(t) = \int G(\Gamma) e^{-\Gamma t} d\Gamma \quad (\text{S1.7})$$

We can now see that the autocorrelation function is a sum of exponential function  $e^{-\Gamma t}$  over a distribution of decay rates  $G(\Gamma)$ .

## Supplementary 2: Optimized field by wavefront shaping and decay rate distribution

We can derive a similar expression for the field obtain after a wavefront optimization if we notice that the field at the target obtained after a wavefront shaping experiment is very similar to the one in equation (S1.2). Assuming an input intensity of unity, we can write [2]:

$$\mathbf{E}_{focus}(\mathbf{t}) = \sqrt{\eta} \sum_m \frac{|E_m|^2}{\langle I \rangle} e^{i\varphi_m(t_m) - i\varphi_m(\mathbf{t})} \quad (\text{S2.1})$$

Where  $\sum_m$  represents the sum over paths aligned in phase by wavefront shaping,  $t_m$  is the time when the phase  $\varphi_m$  was measured and  $\eta$  is the enhancement. If the wavefront shaping process is stopped at time  $t = 0$ , we have for  $t \geq 0$  (with  $t_m < 0$ ).

By defining  $\Delta t_m = t - t_m$  and  $\Delta\varphi_m(\Delta t_m) = \varphi_m(t_m) - \varphi_m(\mathbf{t})$ , we obtain:

$$\mathbf{E}_{focus}(\mathbf{t}) = \sqrt{\eta} \sum_m \frac{|E_m|^2}{\langle I \rangle} e^{i\Delta\varphi_m(\Delta t_m)} \quad (\text{S2.2})$$

As done previously, we can also express the field at the focus in term of decay rates. An extra term appears compared to equation S1.5 which takes into account that the phases aren't measured at the same time:

$$|\mathbf{E}_{focus}(\mathbf{t})| = \sqrt{\eta} \sum_m \frac{|E_m|^2}{\langle I \rangle} e^{-\Gamma_m(t-t_m)} \quad (\text{S2.3})$$

$$|\mathbf{E}_{focus}(\mathbf{t})| = \sqrt{\eta} \sum_m \frac{|E_m|^2}{\langle I \rangle} e^{\Gamma_m t_m} e^{-\Gamma_m t} \quad (\text{S2.4})$$

The term  $e^{\Gamma_m t_m}$  (with  $t_m < 0$ ) indicates that the population of paths decaying with a decay rate  $\Gamma_m$  decreases if the phases associated to these paths were measured a long time before ending the optimization.

Finally, we can recast the expression (S2.6) as a sum over decay rates  $\Gamma$  according to the distribution of decay rates  $G_m$ :

$$|\mathbf{E}_{focus}(\mathbf{t})| = \sqrt{\eta} \sum_{\Gamma} G_m(\Gamma) e^{-\Gamma t} \quad (\text{S2.5})$$

By passing to the continuum limit, we finally obtain:

$$|\mathbf{E}_{focus}(\mathbf{t})| = \sqrt{\eta} \int G_m(\Gamma) e^{-\Gamma t} d\Gamma \quad (\text{S2.6})$$

where  $G_m(\Gamma)$  is the distribution of decay rates present at the focus. It can differ from  $G(\Gamma)$  for two reasons: 1) the optimization process doesn't pick statistically the same path distribution as the speckle and 2) the time when a path is aligned by wavefront shaping is taking into account. Paths with high decay rate will be less present at the end of the optimization.

## References

1. Weitz, D.A.; Pine, D.J. Diffusing Wave Spectroscopy. In Dynamic Light Scattering; Brown, W., Ed.; Oxford University Press: New York, 1993; 652–720.
2. Jang, M., Ruan, H., Vellekoop, I. M., Judkewitz, B., Chung, E., & Yang, C. (2015). Relation between speckle decorrelation and optical phase conjugation (OPC)-based turbidity suppression through dynamic scattering media: a study on in vivo mouse skin. Biomedical optics express, 6(1), 72-85.

# Enhanced stability of the focus obtained by wavefront optimization in dynamical scattering media: supplementary material

BAPTISTE BLOCHET<sup>1,2,\*</sup>, KELLY JOAQUINA<sup>1</sup>, LISA BLUM<sup>1</sup>, LAURENT BOURDIEU<sup>2,†</sup>, SYLVAIN GIGAN<sup>1,†</sup>

<sup>1</sup>Laboratoire Kastler Brossel, UPMC-Sorbonne Universités, ENS-PSL Research University, CNRS, Collège de France ; 24 rue Lhomond, F-75005 Paris, France

<sup>2</sup>IBENS, Département de Biologie, Ecole Normale Supérieure, CNRS, Inserm, PSL Research University, F-75005 Paris, France

<sup>†</sup>Senior author

\*Corresponding author: [baptiste.bloch@lkb.ens.fr](mailto:baptiste.bloch@lkb.ens.fr)

Published XX Month XXXX

This document provides supplementary information to “Enhanced stability of the focus obtained by wavefront optimization in dynamical scattering media”. It shows the derivation of two models to express the autocorrelation function  $g_1$  and the degradation of the focus after wavefront shaping as integrals of exponential decay over decay rate distributions.

<http://dx.doi.org/10.1364/optica.99.099999.s1> [supplementary document doi]

## Supplementary 1: Autocorrelation function and decay rate distribution

Under the diffusion approximation, we can write that the total field at the detector is a superposition of the fields from all light paths through the sample to the detector:

$$E(t) = \sum_p E_p e^{i\varphi_p(t)} \quad (\text{S1.1})$$

where  $\sum_p$  represents the sum over paths,  $E_p$  and  $\varphi_p$  are respectively the amplitude and the phase of the field from path  $p$ .

By assuming that the fields from different paths are uncorrelated, we obtain:

$$g_1(t) \equiv \frac{\langle E(t')E^*(t+t') \rangle}{\langle |E(t)|^2 \rangle} = \sum_p \frac{|E_p|^2}{\langle I \rangle} \langle e^{i\Delta\varphi_p(t)} \rangle \quad (\text{S1.2})$$

Where  $\langle I \rangle$  is the total average scattered intensity at the detector and  $\Delta\varphi_p(t) = \varphi_p(0) - \varphi_p(t)$ . Using the fact that  $\Delta\varphi_p$  is a gaussian random variable, we obtain:

$$\langle e^{i\Delta\varphi_p(t)} \rangle = e^{-\langle \Delta\varphi_p(t)^2 \rangle / 2} \quad (\text{S1.3})$$

For a mixture of colloidal scatterers under Brownian motion, we obtain the following expression [1]:

$$\langle \Delta\varphi_p(t)^2 \rangle = \sum_i 2n_{i,p} \langle q_{i,p}^2 \rangle D_{i,p} t \quad (\text{S1.4})$$

where  $\sum_i$  represents the sum over particle type,  $n_{i,p}$  the number of scattering events from specie  $i$ ,  $\langle q_{i,p}^2 \rangle$  the average over scattering vectors and  $D_{i,p}$  the diffusing constant of the specie  $i$  in the path  $p$ .

We can now express the autocorrelation function in the following way:

$$g_1(t) = \sum_p \frac{|E_p|^2}{\langle I \rangle} e^{-\Gamma_p t} \quad (\text{S1.5})$$

Where  $\Gamma_p = \sum_i 2n_{i,p} \langle q_{i,p}^2 \rangle D_{i,p}$  is the decay rate associated to the path  $p$ . We can recast the last equation as a sum over decay rates  $\Gamma$  rather than a sum over individual paths provided that we replace the fraction of scattered intensity in path  $p$ :  $|E_p|^2 / \langle I \rangle$ , with the distribution of decay rates  $G(\Gamma)$ :

$$g_1(t) = \sum_\Gamma G(\Gamma) e^{-\Gamma t} \quad (\text{S1.6})$$

By passing to the continuum limit, we finally obtain:

$$g_1(t) = \int G(\Gamma) e^{-\Gamma t} d\Gamma \quad (\text{S1.7})$$

We can now see that the autocorrelation function is a sum of exponential function  $e^{-\Gamma t}$  over a distribution of decay rates  $G(\Gamma)$ .

## Supplementary 2: Optimized field by wavefront shaping and decay rate distribution

We can derive a similar expression for the field obtain after a wavefront optimization if we notice that the field at the target obtained after a wavefront shaping experiment is very similar to the one in equation (S1.2). Assuming an input intensity of unity, we can write [2]:

$$\mathbf{E}_{focus}(\mathbf{t}) = \sqrt{\eta} \sum_m \frac{|E_m|^2}{\langle I \rangle} e^{i\varphi_m(t_m) - i\varphi_m(\mathbf{t})} \quad (\text{S2.1})$$

Where  $\sum_m$  represents the sum over paths aligned in phase by wavefront shaping,  $t_m$  is the time when the phase  $\varphi_m$  was measured and  $\eta$  is the enhancement. If the wavefront shaping process is stopped at time  $t = 0$ , we have for  $t \geq 0$  (with  $t_m < 0$ ).

By defining  $\Delta t_m = t - t_m$  and  $\Delta\varphi_m(\Delta t_m) = \varphi_m(t_m) - \varphi_m(\mathbf{t})$ , we obtain:

$$\mathbf{E}_{focus}(\mathbf{t}) = \sqrt{\eta} \sum_m \frac{|E_m|^2}{\langle I \rangle} e^{i\Delta\varphi_m(\Delta t_m)} \quad (\text{S2.2})$$

As done previously, we can also express the field at the focus in term of decay rates. An extra term appears compared to equation S1.5 which takes into account that the phases aren't measured at the same time:

$$|\mathbf{E}_{focus}(\mathbf{t})| = \sqrt{\eta} \sum_m \frac{|E_m|^2}{\langle I \rangle} e^{-\Gamma_m(t-t_m)} \quad (\text{S2.3})$$

$$|\mathbf{E}_{focus}(\mathbf{t})| = \sqrt{\eta} \sum_m \frac{|E_m|^2}{\langle I \rangle} e^{\Gamma_m t_m} e^{-\Gamma_m t} \quad (\text{S2.4})$$

The term  $e^{\Gamma_m t_m}$  (with  $t_m < 0$ ) indicates that the population of paths decaying with a decay rate  $\Gamma_m$  decreases if the phases associated to these paths were measured a long time before ending the optimization.

Finally, we can recast the expression (S2.6) as a sum over decay rates  $\Gamma$  according to the distribution of decay rates  $G_m$ :

$$|\mathbf{E}_{focus}(\mathbf{t})| = \sqrt{\eta} \sum_{\Gamma} G_m(\Gamma) e^{-\Gamma t} \quad (\text{S2.5})$$

By passing to the continuum limit, we finally obtain:

$$|\mathbf{E}_{focus}(\mathbf{t})| = \sqrt{\eta} \int G_m(\Gamma) e^{-\Gamma t} d\Gamma \quad (\text{S2.6})$$

where  $G_m(\Gamma)$  is the distribution of decay rates present at the focus. It can differ from  $G(\Gamma)$  for two reasons: 1) the optimization process doesn't pick statistically the same path distribution as the speckle and 2) the time when a path is aligned by wavefront shaping is taking into account. Paths with high decay rate will be less present at the end of the optimization.

## References

1. Weitz, D.A.; Pine, D.J. Diffusing Wave Spectroscopy. In Dynamic Light Scattering; Brown, W., Ed.; Oxford University Press: New York, 1993; 652–720.
2. Jang, M., Ruan, H., Vellekoop, I. M., Judkewitz, B., Chung, E., & Yang, C. (2015). Relation between speckle decorrelation and optical phase conjugation (OPC)-based turbidity suppression through dynamic scattering media: a study on in vivo mouse skin. Biomedical optics express, 6(1), 72-85.